

Supporting Information

## **Silver-Copper Nanoalloy Catalyst Layer for Bifunctional Air Electrodes in Alkaline Media**

Xiaoqiang Wu <sup>a</sup>, Fuyi Chen<sup>\*,a</sup>, Yachao Jin <sup>a</sup>, Nan Zhang <sup>a</sup> and Roy L. Johnston <sup>\*,b</sup>

<sup>a</sup> State Key Laboratory of Solidification Processing, Northwestern Polytechnic

University, Xian, 710072, China

<sup>b</sup> Department of Chemistry, University of Birmingham, Birmingham, B15 2TT, U.K.

\*Corresponding author. fuyichen@nwpu.edu.cn (Fuyi Chen).

r.l.johnston@bham.ac.uk (Roy L. Johnston)

## Contents

|   |           |
|---|-----------|
| 1. Model and computational methods.   | Page S-3  |
| 2. Rechargeable Zn-air battery construction and mechanism of the rechargeable Zn-air battery  | Page S-3  |
| Figure S1. (a) TEM images and the particle size distribution of Ag-Cu nanoparticles in the film. (b-d)TEM images after 200 cycling. (e) STEM-HAADF line scan (EDS) of the Ag <sub>50</sub> Cu <sub>50</sub> film on nickel grid.  | Page S-5  |
| Figure S2. (a) ORR polarization curves of Ag/Ni. (b) Comparison Koutecky-Levich plots collected from the ORR for Ag/Ni respectively.  | Page S-6  |
| Figure S3. (a) ORR polarization curves of Ag <sub>25</sub> Cu <sub>75</sub> /Ni. (b) Koutecky-Levich plots collected from the ORR for Ag <sub>25</sub> Cu <sub>75</sub> /Ni respectively. (c) Koutecky-Levich plots for Ag, Ag <sub>90</sub> Cu <sub>10</sub> , Ag <sub>50</sub> Cu <sub>50</sub> and Ag <sub>25</sub> Cu <sub>75</sub> . | Page S-7  |
| Figure S4. (a) The curves of cycle for secondary zinc-air battery at 20 mA cm <sup>-2</sup> for 200 cycles in 6M KOH+ 0.1M Zn(CH <sub>3</sub> COO) <sub>2</sub> solution.   | Page S-8  |
| Figure S5. The gas-tight zinc-air battery for the measurement of the electrolyte decomposition. The gas evolution is measured by gas chromatography (GC7980) with thermal conductivity detection (TCD).   | Page S-9  |
| Figure S6. The chromatographic response for O <sub>2</sub> , when air pour into the Inlet and out of the outlet during the discharging processing: (a-b) at the start of discharging. (c-d) after 1hour discharging.  | Page S-10 |
| Figure S7. The chromatographic response for O <sub>2</sub> inlet and outlet of the battery during charging process.   | Page S-11 |
| Table S1. Parameters of Koutecky-Levich plots collected from the ORR for pure Ag.   | Page S-12 |
| Table S2. Parameters of Koutecky-Levich plots from the ORR for Ag <sub>90</sub> Cu <sub>10</sub>  | Page S-12 |
| Table S3. Parameters of Koutecky-Levich plots from the ORR for Ag <sub>50</sub> Cu <sub>50</sub>  | Page S-13 |
| Table S4. Parameters of Koutecky-Levich plots from the ORR for Ag <sub>25</sub> Cu <sub>75</sub>  | Page S-13 |
| Table S5. Comparison of air catalysts for zinc-air batteries.   | Page S-14 |

## **1. Model and computational methods**

The electronic structures and adsorption geometries of O<sub>2</sub> or O on Ag<sub>12</sub>Cu nanoclusters were investigated using first-principles calculation that are based on density functional spin-polarized theory. The Kohn–Sham equation was expanded in a double-numerical quality basis set with polarization functions (DNP), and the revised PBE (RPBE) exchange correlation functional was utilized. The RPBE functional is superior in the description of the energetics of atomic and molecular bonding on transition metals. The orbital cutoff range was set to 5.0 Å and the Fermi smearing was set to 0.002 Ha. The DFT semi-core pseudo potential was used to treat the core electrons of heavy Ag and Cu atoms. The convergence tolerances of energies, forces and displacements were  $1.0 \times 10^{-5}$  Ha, 0.002 Ha/Å and 0.005 Å, respectively.

## **2. Rechargeable Zn-air battery construction and mechanism of the rechargeable Zn-air battery**

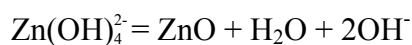
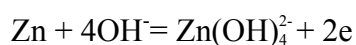
The single-chamber rechargeable zn-air batteries were constructed with an inner cylinder chamber 3 cm in diameter and an electrode spacing of 4 cm (Figure S5). The negative electrode is the zinc plate, which was polished and cleaned in distilled water before use. The positive electrode is the air cathode. As shown in table of contents , the air cathodes consisted of a current collector with a gas diffusion layer (GDL) and a catalyst layer (CL). The collector was made by the nickel foam, the GDL was prepared by carbon black and PTFE with a mass ratio of 3:7. The catalyst or CL was deposited by PLD (as noted in the experiment section). To make an air cathode, the GDL was placed on the backside of a collector, which was free of the catalyst layer, and was

pressed into a 0.5-mm-thick layer by a rolling machine. The prepared cathodes were dried at 50 °C for 5 hours to get rid of the water and alcohol in a vacuum oven, and then heat-treated on the hot plate at 200 °C for 5 min.

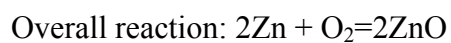
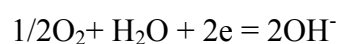
The electrochemical reactions that occur in rechargeable Zn-air system with alkaline electrolyte are as follows:

(1) Discharge

Zinc plate (negative electrode):

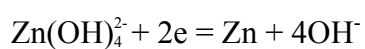
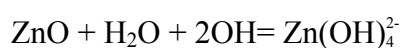


Air electrode (positive electrode):

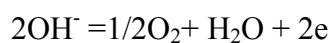


(2) Charge

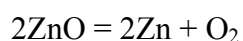
Zinc plate (cathode):



Air electrode (anode):



Overall reaction:



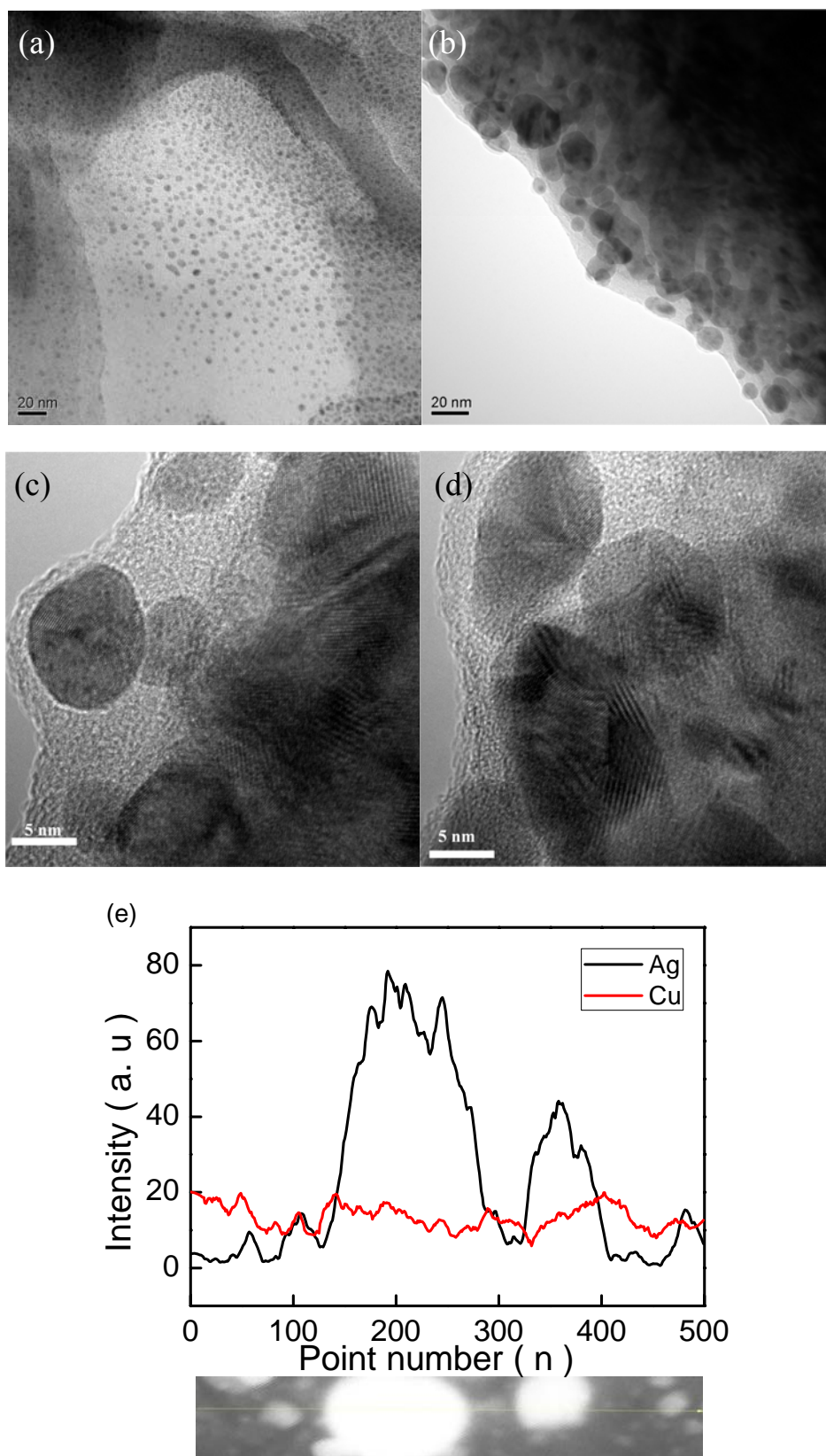


Figure S1. (a) TEM images and the particle size distribution of Ag-Cu nanoparticles in the film. (b-d) TEM images after 200 cycling. (e) STEM-HAADF line scan (EDS) of the  $\text{Ag}_{50}\text{Cu}_{50}$  film on nickel grid.

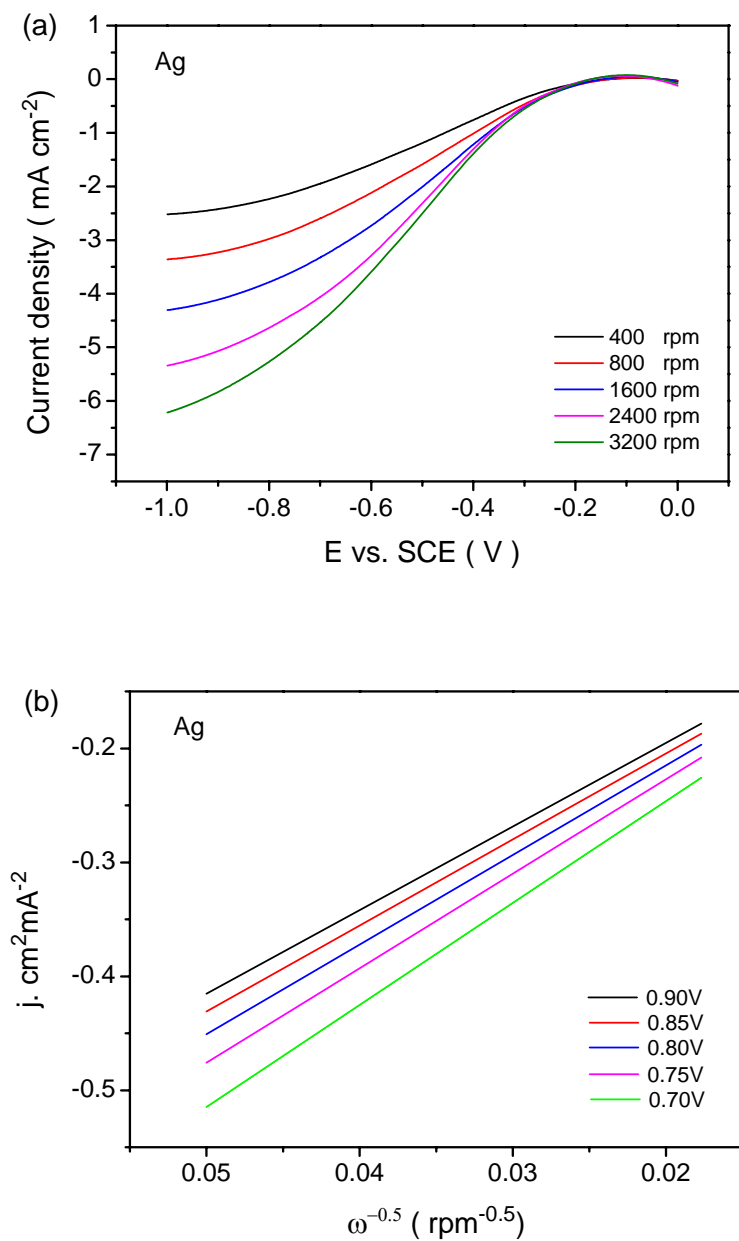


Figure S2. (a) ORR polarization curves of Ag/Ni. (b) Comparison Koutecky-Levich plots collected from the ORR for Ag/Ni respectively.

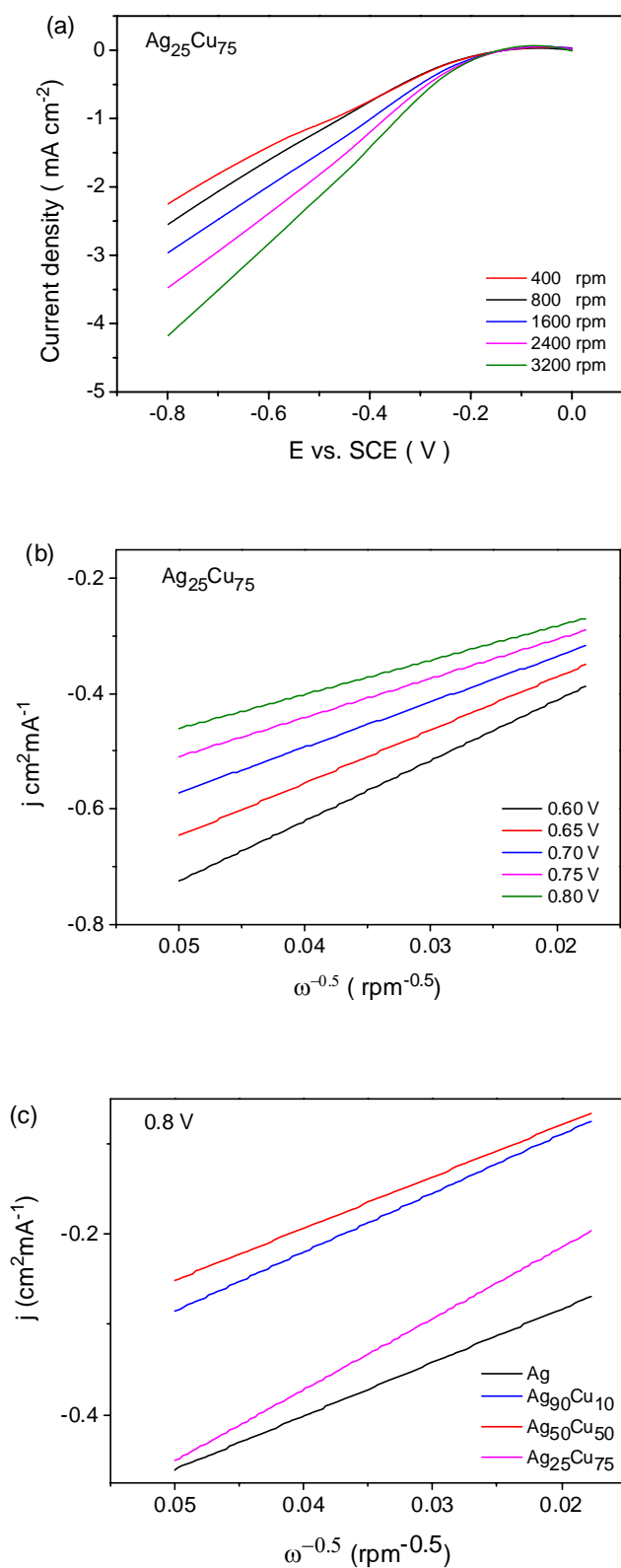


Figure S3. (a) ORR polarization curves of  $\text{Ag}_{25}\text{Cu}_{75}$ /Ni. (b) Koutecky-Levich plots collected from the ORR for  $\text{Ag}_{25}\text{Cu}_{75}$ /Ni respectively. (c) Koutecky-Levich plots for Ag,  $\text{Ag}_{90}\text{Cu}_{10}$ ,  $\text{Ag}_{50}\text{Cu}_{50}$  and  $\text{Ag}_{25}\text{Cu}_{75}$ .

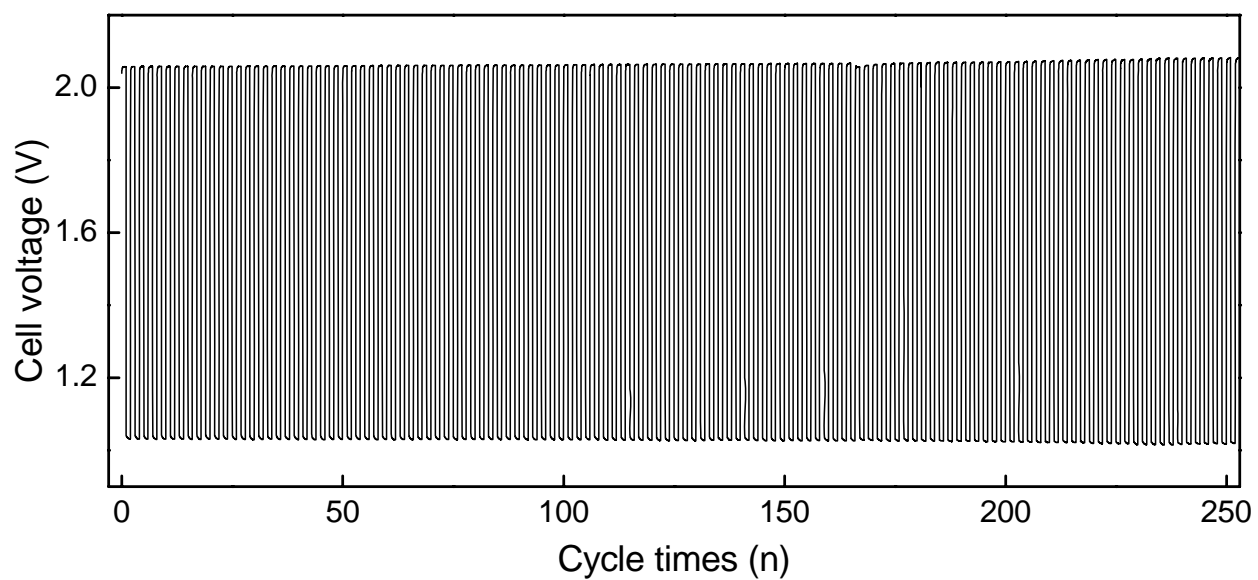


Figure S4. The curves of cycle for secondary zinc-air battery at  $20 \text{ mA cm}^{-2}$  for 200 cycles in 6M KOH+ 0.1M  $\text{Zn}(\text{CH}_3\text{COO})_2$  solution.





Figure S5. The gas-tight zinc-air battery for the measurement of the electrolyte decomposition. The gas evolution is measured by gas chromatography (GC7980) with thermal conductivity detection (TCD).

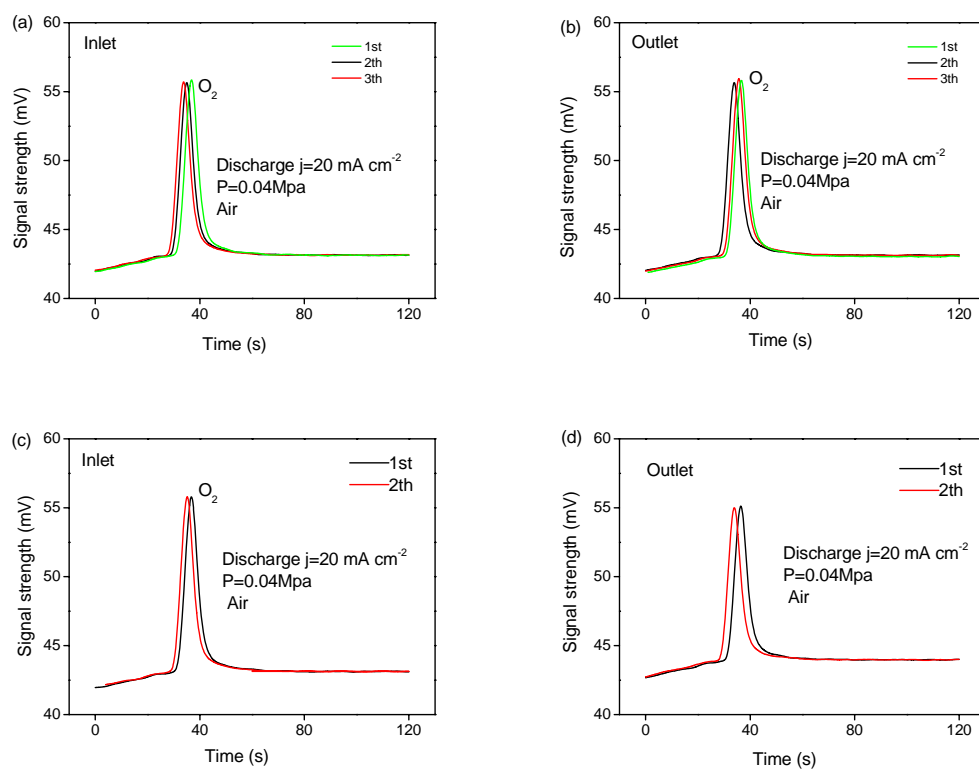


Figure S6. The chromatographic response for  $O_2$ , when air pour into the Inlet and out of the outlet during the discharging processing: (a-b) at the start of discharging. (c-d) after 1 hour discharging.

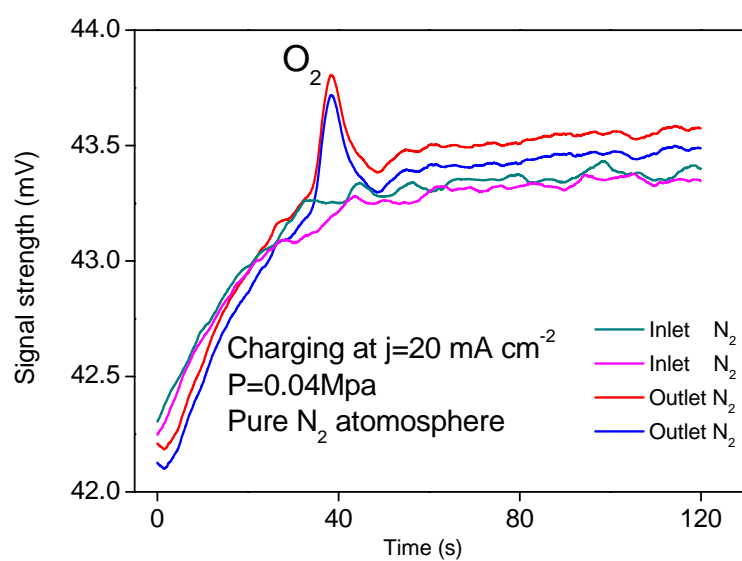


Figure S7. The chromatographic response for  $\text{O}_2$  inlet and outlet of the battery during charging process.

Table S1. Parameters of Koutecky-Levich plots collected from the ORR for pure Ag

| Ag                                  | 0.70V |       | 0.75V |       | 0.80V |       | 0.85V |       | 0.90V |       |
|-------------------------------------|-------|-------|-------|-------|-------|-------|-------|-------|-------|-------|
| $\omega^{-0.5}$ rpm <sup>-0.5</sup> | j     | 1/j   | j     | 1/j   | j     | 1/j   | j     | 1/j   | j     | 1/j   |
| 0.05                                | -2.01 | -0.51 | -2.11 | -0.47 | -2.23 | -0.45 | -2.34 | -0.43 | -2.42 | -0.41 |
| 0.03536                             | -2.60 | -0.38 | -2.82 | -0.36 | -2.97 | -0.34 | -3.11 | -0.32 | -3.23 | -0.39 |
| 0.025                               | -3.34 | -0.30 | -3.59 | -0.28 | -3.78 | -0.27 | -3.96 | -0.25 | -4.11 | -0.24 |
| 0.0204                              | -4.06 | -0.25 | -4.39 | -0.23 | -4.62 | -0.22 | -4.86 | -0.21 | -5.72 | -0.20 |
| 0.0177                              | -4.51 | -0.22 | -4.94 | -0.20 | -5.27 | -0.19 | -5.55 | -0.18 | -5.83 | -0.17 |

Table S2. Parameters of Koutecky-Levich plots from the ORR for Ag<sub>90</sub>Cu<sub>10</sub>

| Ag <sub>90</sub> Cu <sub>10</sub>   | 0.60V |       | 0.65V  |       | 0.70V  |       | 0.75V  |       | 0.80V  |       |
|-------------------------------------|-------|-------|--------|-------|--------|-------|--------|-------|--------|-------|
| $\omega^{-0.5}$ rpm <sup>-0.5</sup> | j     | 1/j   | j      | 1/j   | j      | 1/j   | j      | 1/j   | j      | 1/j   |
| 0.05                                | -2.99 | -0.33 | -3.10  | -0.32 | -3.18  | -0.31 | -3.27  | -0.31 | -3.37  | -0.30 |
| 0.03536                             | -5.20 | -0.19 | -5.43  | -0.18 | -5.61  | -0.18 | -5.72  | -0.17 | -5.80  | -0.17 |
| 0.025                               | -7.70 | -0.13 | -8.05  | -0.12 | -8.37  | -0.12 | -8.62  | -0.12 | -8.84  | -0.11 |
| 0.0204                              | -9.13 | -0.11 | -9.54  | -0.11 | -9.92  | -0.10 | -10.23 | -0.10 | -10.56 | -0.10 |
| 0.0177                              | -9.74 | -0.10 | -10.33 | -0.09 | -10.83 | -0.09 | -11.16 | -0.09 | -11.43 | -0.09 |

Table S3. Parameters of Koutecky-Levich plots from the ORR for Ag<sub>50</sub>Cu<sub>50</sub>

| Ag <sub>50</sub> Cu <sub>50</sub>  | 0.60V  |       | 0.65V  |       | 0.70V  |       | 0.75V  |       | 0.80V  |       |
|------------------------------------|--------|-------|--------|-------|--------|-------|--------|-------|--------|-------|
| $\omega^{-0.5} \text{ rpm}^{-0.5}$ | j      | 1/j   | j      | 1/j   | j      | 1/j   | j      | 1/j   | j      | 1/j   |
| 0.05                               | -3.09  | -0.34 | -3.15  | -0.32 | -3.24  | -0.31 | -3.38  | -0.31 | -3.45  | -0.30 |
| 0.03536                            | -5.88  | -0.17 | -6.12  | -0.16 | -6.34  | -0.16 | -6.48  | -0.15 | -6.56  | -0.15 |
| 0.025                              | -8.69  | -0.12 | -9.08  | -0.11 | -9.46  | -0.11 | -9.74  | -0.10 | -9.99  | -0.10 |
| 0.0204                             | -10.34 | -0.10 | -10.72 | -0.09 | -11.19 | -0.09 | -11.56 | -0.09 | -11.93 | -0.08 |
| 0.0177                             | -11.03 | -0.09 | -11.61 | -0.08 | -12.41 | -0.07 | -12.83 | -0.08 | -13.23 | -0.08 |

Table S4. Parameters of Koutecky-Levich plots from the ORR for Ag<sub>25</sub>Cu<sub>75</sub>

| Ag <sub>25</sub> Cu <sub>75</sub>  | 0.60V |       | 0.65V |       | 0.70V |       | 0.75V |       | 0.80V |       |
|------------------------------------|-------|-------|-------|-------|-------|-------|-------|-------|-------|-------|
| $\omega^{-0.5} \text{ rpm}^{-0.5}$ | j     | 1/j   | j     | 1/j   | j     | 1/j   | j     | 1/j   | j     | 1/j   |
| 0.05                               | -1.42 | -0.70 | -1.60 | -0.62 | -1.81 | -0.55 | -2.04 | -0.49 | -2.12 | -0.47 |
| 0.03536                            | -1.62 | -0.60 | -1.84 | -0.54 | -2.08 | -0.48 | -2.31 | -0.43 | -2.55 | -0.39 |
| 0.025                              | -2.01 | -0.50 | -2.24 | -0.45 | -2.48 | -0.40 | -2.74 | -0.37 | -2.96 | -0.34 |
| 0.0204                             | -2.41 | -0.42 | -2.67 | -0.37 | -2.95 | -0.34 | -3.23 | -0.31 | -3.47 | -0.29 |
| 0.0177                             | -2.86 | -0.35 | -3.18 | -0.31 | -3.51 | -0.28 | -3.87 | -0.26 | -4.38 | -0.22 |

Table S5. Comparison of air catalysts for zinc-air batteries.

| Catalysts  | Electrolytes | Primary battery |                | Rechargeable battery |                |                |                |                | Ref.      |
|--|--------------|-----------------|----------------|----------------------|----------------|----------------|----------------|----------------|-----------|
|  |              | I <sup>a</sup>  | W <sup>b</sup> | I <sup>c</sup>       | V <sup>d</sup> | V <sup>e</sup> | N <sup>f</sup> | R <sup>g</sup> |           |
| Ag-Cu/Ni*  | 6 M KOH      | 60              | 86.3           | 20                   | 2.2            | 1.08           | 200            | 0.01           | This work |
| Ag/C   | 6.5 M KOH    | 15              | 34             |                      |                |                |                |                | 1         |
| MnO <sub>2</sub> /C                              | 7 M KOH      | 40              | 95             |                      |                |                |                |                | 2         |
| N-doped CNTs                                     | 6 M KOH      | 50              | 70             |                      |                |                |                |                | 3         |
| MnO <sub>2</sub> -NCNT                           | 6 M KOH      | 20              |                | 20                   | 2.6            | 1.0            | 50             | 0.3            | 4         |
| MnO <sub>2</sub> -Co <sub>3</sub> O <sub>4</sub> | 6 M KOH      | 15              |                | 15                   | 2.3            | 1.1            | 60             | 0.3            | 5         |
| NiCo <sub>2</sub> O <sub>4</sub>                 | 6 M KOH      | 20              |                | 20                   | 1.8            | 1.1            | 40             | 0.1            | 6         |
| La <sub>2</sub> NiO <sub>4</sub>                 | 6 M KOH      | 25              |                | 25                   | 1.5            | 1.1            | 40             | 0.1            | 7         |

\*The battery performance was measured in the natural air.

<sup>a</sup> The discharge current density (mA cm<sup>-2</sup>) at 1V,

<sup>b</sup> The peak power density (mW cm<sup>-2</sup>) of the primary battery,

<sup>c</sup> The working current density (mA m<sup>-2</sup>) used for the charging and discharging test,

<sup>d</sup> The cell voltage (V) in charging process at the working current density,

<sup>e</sup> The cell voltage (V) in discharging process at the working current density,

<sup>f</sup> The cycle numbers (N) of the recharge battery at the working current density,

<sup>g</sup> The polarization increased (R) refer to difference between charge and discharge voltage at the end.

## References

- (1) Han, J. J.; Li, N.; Zhang, T. Y. Ag/C Nanoparticles as an Cathode Catalyst for a Zinc-Air Battery with a Flowing Alkaline Electrolyte. *J. Power Sources* **2009**, *193*, 885-889.
- (2) Wei, Z. D.; Huang, W. Z.; Zhang, S. T.; Tan, J. Carbon-Based Air Electrodes Carrying MnO<sub>2</sub> in Zinc-air Batteries. *J. Power Sources* **2000**, *91*, 83-85.
- (3) Zhu, S. M.; Chen, Z.; Li, B.; Higgins, D.; Wang, H. J.; Li, H.; Chen, Z. W. Nitrogen-Doped Carbon Nanotubes as Air Cathode Catalysts in Zinc-Air Battery. *Electrochim. Acta* **2011**, *56*, 5080-5084.
- (4) Chen, Z.; Yu, A.; Ahmed, R.; Wang, H.; Li, H.; Chen, Z. Manganese Dioxide Nanotube and Nitrogen-Doped Carbon Nanotube Based Composite Bifunctional Catalyst for Rechargeable Zinc-air Battery. *Electrochim. Acta* **2012**, *69*, 295-300.
- (5) Du, G. J.; Liu, X. G.; Zong, Y.; Hor, T. S. A.; Yu, A. S.; Liu, Z. L. Co<sub>3</sub>O<sub>4</sub> Nanoparticle-Modified MnO<sub>2</sub> Nanotube Bifunctional Oxygen Cathode Catalysts for Rechargeable Zinc-Air Batteries. *Nanoscale* **2013**, *5*, 4657-4661.
- (6) Prabu, M.; Ketpang, K.; Shanmugam, S. Hierarchical Nanostructured NiCo<sub>2</sub>O<sub>4</sub> as an Efficient Bifunctional Non-precious Metal Catalyst for Rechargeable Zinc-Air Batteries. *Nanoscale* **2014**, *6*, 3173-3181.
- (7) Jung, K. N.; Jung, J. H.; Im, W. B.; Yoon, S.; Shin, K. H.; Lee, J. W. Doped Lanthanum Nickelates with a Layered Perovskite Structure as Bifunctional Cathode Catalysts for Rechargeable Metal-Air Batteries. *ACS Appl. Mater. Interfaces* **2013**, *5*, 9902-9907.